Electron-spin-resonance STM on iron atoms in silicon

Y. Manassen, I. Mukhopadhyay, and N. Ramesh Rao
Department of Physics, Ben Gurion University, P.O. Box 653 Be'er Sheva 84105, Israel
(Received 12 October 1999)

Electron-spin-resonance–scanning tunneling microscopy (ESR)-(STM) of iron atoms in silicon was observed: Si(111) surfaces were covered with iron atoms and annealed. This gives surfaces covered with small islands of different silicide phases. We could detect an ESR-STM signal that corresponds to a g value of 2.07. The signal was split by magnetic field modulation, and phase-sensitive detection was applied. This shows that electron-spin-resonance (ESR)-STM signals can be detected on a surface that is imaged with atomic resolution and that it is possible to observe a $g \neq 2$ spin center. Getting absorption (instead of the expected derivative) line shapes with phase-sensitive detection is explained by the asymmetry in the line shape, which is a result of a rapid scan of the signal. Then, when the integration time of the phase sensitive detector is close to the time it takes to sweep the linewidth of the signal, absorption line shapes are observed.

I. INTRODUCTION

It is widely accepted that the upper sensitivity in conventional (cw X band) ESR (electron spin resonance) is 10^{10} electron spins. This relatively low sensitivity is basically due to the fact that only a fraction (determined by the Boltzmann factor) of spins is actually detected, and to the inefficient method of detection. There is no physical limit to improving it by many orders of magnitude.

It was shown in the past that it is possible to improve the sensitivity of spin detection to an extent that single spins can be detected. Techniques that are based on single molecule ODMR spectroscopy were proved to be capable of single spin detection.[1–3] A technique that is based on mechanical detection of magnetic resonance[4] with an atomic force microscope is approaching single spin sensitivity. However, both methods give no information on the spatial position of the observed spin in the sample. Electron-spin-resonance (ESR)-STM,[5–7] on the other hand, is an STM (scanning tunneling microscope) based technique. The extremely local nature of STM based measurements suggests that electron-spin-resonance (ESR)-STM also has single spin sensitivity. While the claim that it can detect a single spin (and not a few spins together) still has to be proved, it offers a capability to correlate between the spectroscopic information and the topography observed at the atomic scale.

The electron-spin-resonance (ESR)-STM experiment was performed with a UHV STM in the presence of an external magnetic field. It was found that when the small tip-sample tunneling junction includes a paramagnetic atom (or atoms), the tunneling current is modulated at the Larmor frequency and rf currents appear there. The experiment was first tried on the Si/SiO_2 system and the rf current was found to be spatially localized with a frequency proportional to the magnetic field. In this system, the spin centers were prepared by thermal oxidation of a clean silicon wafer. The spin centers are Si radicals known as P_b centers. They are located at the Si/SiO_2 interface. The dependence of the frequency of the signal on the magnetic field was shown in real time.[7] Although the reality of this effect was proved beyond a doubt, several crucial questions still remained unsolved. For example, the Si/SiO_2 system is not an optimal system as far as resolution is concerned. Is it possible to observe electron-spin-resonance (ESR)-STM signals from a surface simultanously with atomic resolution? The Si/SiO_2 spin centers have a g value close to 2. However, looking at this frequency leaves doubts regarding the interpretation of the signals as originated from the Si radicals at the Si/SiO_2 interface, since this can be also related to free or trapped electrons, etc. In other words Is it possible to observe signals with a frequency corresponding to $g \neq 2$?

Other questions are related to the unusual detection scheme that was used in order to detect electron-spin-resonance (ESR)-STM signals: It consists of an impedance matching circuit, a spectrum analyzer, and a phase sensitive detector (lock-in amplifier). In a previous paper[7] we explained how such a detection system should lead to a derivative line shape from the phase-sensitive detector. However, this is not in accord with the fact that in many experiments, absorption line shapes are observed with the phase-sensitive detector. This includes electron-spin-resonance (ESR)-STM work on a paramagnetic molecule.[8]

In this paper we try to resolve all these questions. We find that the iron-doped silicon system can be a good system to answer them. We show that indeed, the signals can be observed on surfaces simultanously with an atomic resolution topographic image. We show that spectroscopic ESR information can be observed by looking at $g \neq 2$ spin centers. The problem of the ocassional observation of nonderivative line shapes with the phase-sensitive detector, in both the Si/SiO_2 and the Fe in silicon systems, is resolved by showing that when a time-dependent signal with a finite lifetime is detected with such a detection scheme, the line shape may change to absorption, if certain detection parameters are used. This is a result of the asymmetry introduced into the line shape as a result of a rapid sweep.

The interstitial iron spin centers in silicon[9] was studied in many ESR experiments. Neutral iron is a fast diffusing element in silicon at high temperatures. The preferential position of iron is in a tetrahedral interstitial site, where it is immobilized in room temperature. The electron configuration is $3d$.[8] The ESR spectrum of this spin center consists of a

single line with a g value of 2.07. Although it is in a tetrahedral site, it was found that the crystal field at the interstitial site is mainly determined by the next-nearest-neighbor atoms, which are arranged in a regular octahedron. The ground state is an orbital singlet with $S=1$.

In the case of exact cubic symmetry, the $-1\leftrightarrow 0$ and $0\leftrightarrow 1$ transitions are degenerate. This degeneracy can be removed by stress, which reduces the symmetry of the site. In the case of a uniaxial stress, the line is split into two. However, the split is anisotropic. For example, it is negligible when applied in the $\langle 111\rangle$ direction.[10] When the stress is not uniaxial, it causes line broadening. The width of this line was used several times in order to measure the stresses induced in silicon as a result of different processes, such as thermal oxidation or introducing doping atoms.

It should be emphasized, however, that these studies were done on a silicon wafer that was doped by Fe atoms, distributed randomly in the bulk of the silicon crystal. In principle, one has to take iron doped silicon and try to observe the $g=2.07$ signal on this surface. The problem is that the probability of hitting an iron atom in such a sample is small. Therefore, one has to adopt the alternative attitude of evaporating iron on a clean silicon surface, and then annealing the sample. In this way, the iron atoms are distributed near the surface of the sample. The point is that they induce the formation of iron silicides, epitaxially grown on the surface. In our experiment we used Si wafers with a (111) orientation.

Several STM studies were performed on iron silicides, epitaxially grown on silicon surfaces.[11–13] In the bulk, the most stable silicide is β-$FeSi_2$. This is a semiconductor material with a direct band gap of 0.87 eV. The structure of β-$FeSi_2$ is orthorhombic with dimensions of ($a=0.986$ nm, $b=0.779$, $c=0.783$). Despite its stability, β-$FeSi_2$ is very hard to grow on Si(111) because of the large lattice mismatch with the Si(111) lattice. Therefore, it was theoretically predicted[14] that another phase of $FeSi_2$ with a fluorite structure would have a metallic character and a lattice parameter of $a=0.5389$ nm and be formed on a Si(111) substrate. This phase has less than 1% mismatch with a Si(111). This metallic fluorite structure was named γ-$FeSi_2$. STM studies showed that this metastable phase can be grown on the Si(111) surface, and that the surface structure is a hexagonal close-packed symmetry with a 2×2 periodicity with respect to the Si(111)1×1 lattice.

The question relevant to the present paper is what is the local structure around the Fe atoms at the $FeSi_2$ surface? An STM study showed that when transition metal atoms are deposited on the Si(111)7×7 surface, the metal atoms occupy near surface tetrahedral interstitial sites.[15] The structure of both β-$FeSi_2$ and γ-$FeSi_2$ is such that the iron atoms in the second layer from the surface (the top layer is made of silicon atoms) occupy sites that have a distorted tetrahedral structure.[16] An ESR study of bulk β-$FeSi_2$ was performed.[17] It showed that in the bulk, the simple ESR spectrum of iron in silicon is complicated by the fine structure terms that result from the removal of the tetrahedral symmetry and the exchange interactions between the spin centers. Nevertheless, in a small cluster on the surface, these effects are expected to be smaller. In principle, the study of a spectrum can provide much information on the particular nanocluster that is investigated. As a result, it was reasonable to expect that some of the small iron silicide clusters on the Si(111)7×7 surface will give a signal at $g=2.07$, as indeed was observed. However, the possibility that this is only part of a more complicated spectrum, cannot be excluded.

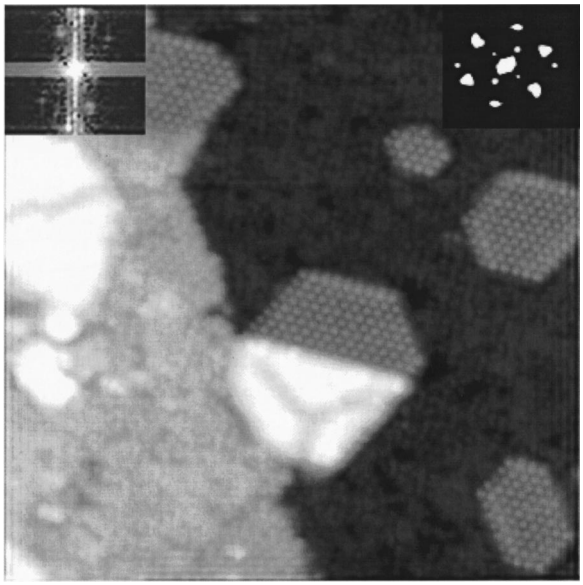

FIG. 1. A typical image of a Si(111) surface after iron deposition and annealing. The image size is 40 nm^2. The island in the center (shown in Fig. 2) is half β-$FeSi_2$ (the lower part) and half γ-$FeSi_2$. The insets in the upper-left and upper-right corners are Fourier transforms of these lower and upper parts, respectively.

II. RESULTS

The experiment was performed with a custom-made UHV-STM with a manual approach mechanism. The magnetic field was induced by two bar magnets that were put on the STM. The magnets induced a magnetic field parallel to the tip. A silicon wafer with a (111) orientation was put in the vacuum chamber, after rinsing with several organic solvents (trichloroethylene, acetone, methanol, and dionized water—in this order). After prolonged heating at 900 °C, the sample was heated to 1200 °C for 1 s—to get rid of the oxide and to induce the 7×7 reconstruction. By low-energy electron diffraction we could verify that 5–10 flashes are sufficient to induce the reconstruction. Afterwards, variable amounts of Fe (from 0.05 to 5 ML) of iron were deposited on the clean surface (we could not find a certain coverage that gives preferable results). Annealing for 3 min at a temperature of 450 °C gave a surface that is covered by iron silicide islands.

Figure 1 shows an image of a typical surface that is observed. The surface is covered by several islands with a diameter of 35–100 nm. The surface in between the islands is either at a clean or a partially disordered 7×7 structure (Fig. 1). Most of the islands have a 2×2 reconstruction that can be easily identified as the γ-$FeSi_2$ phase. The island in the center of Fig. 1 is special in that it is made of two equal halves of two different phases. While the 2×2 reconstruction in the upper half is characteristic to the γ-$FeSi_2$ phase, imaging the lower half of the island does not give atomic resolution information. Nevertheless, we could identify the

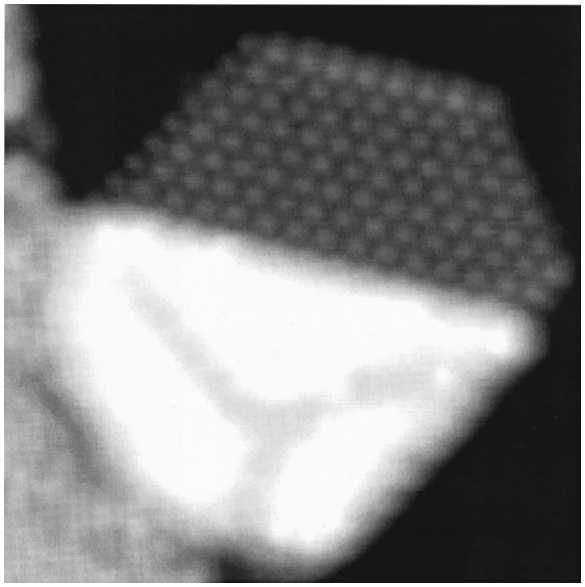

FIG. 2. An enlarged part of the central island in the image of Fig. 1, showing an island that is half γ-$FeSi_2$ and half β-$FeSi_2$. The image size is 10 nm^2.

structure of this half using a Fourier transform of this part of the image (shown in the inset in the upper-left corner) and comparing it with the Fourier transform of the 2×2 part (shown in the inset of the upper-right corner). By using the size and the direction of the vectors of the 2×2 unit cell, it was possible to find that the unit vectors of the rectangular unit cell shown in the left inset are 1.26 and 0.78 nm in length. This is precisely the size of the β-$FeSi_2$(101) unit cell.[13] Figure 2 shows the half γ-$FeSi_2$, half β-$FeSi_2$ island on a larger scale. No atomic resolution is seen in real space in the β-$FeSi_2$ part of the island, but it is possible to see three prolonged depressions extending from the center of this part to its edges. These depressions are a result of the large epitaxial mismatch between the Si(111) substrate and the β-$FeSi_2$. Similar depressions appear in many other islands in the surface (one such island is shown in the left of Fig. 1). They are clearly characteristic to small β-$FeSi_2$ islands. One can see from these and other images that β-$FeSi_2$ can be grown on Si(111) as long as the island is small enough.

It is possible to explain the appearance of these depressions in terms of the superstructure formed when β-$FeSi_2$(101) is grown epitaxially on Si(111). What had probably occurred is that initially the deposition was done on a Si(111) 7×7 surface. On the reconstructed surface, the constraints on the growth of the β-$FeSi_2$ do not exist, and therefore small β-$FeSi_2$ islands are formed. However, since the substrate under the island is covered, it is converted to the unreconstructed structure. At this moment, the stress induced by the (111) surface, converts the β-$FeSi_2$ to γ-$FeSi_2$. The island shown in Fig. 2 is in the middle of this conversion process. Details about this will be published elsewhere.[18] Our electron-spin-resonance (ESR)-STM measurements were mostly done on $FeSi_2$ islands.

The electron-spin-resonance (ESR)-STM measurements were performed at a magnetic field of approximately 150 G. The exact value of the field was determined precisely before each experiment with a Gauss meter. The sample bias voltage was 0.33 V. Unless otherwise stated, the tunneling current was 1 nA. Although the signals appeared to be weaker as compared to measurements on the Si/SiO_2 system, they could be observed with a spectrum analyzer alone (namely, without phase-sensitive detection). The motivation for doing this is that, as will be shown later, line shapes that are observed from a phase-sensitive detector, are not always reliable indicators for the real line shape. Therefore, if one wants to learn something from the line shape, it is better to look directly at the spectrum analyzer. Our first aim was to show, in a similar way as was done in Fig. 1 of Ref. 7 for the Si/SiO_2 system, that the line shape is affected by magnetic-field modulation.

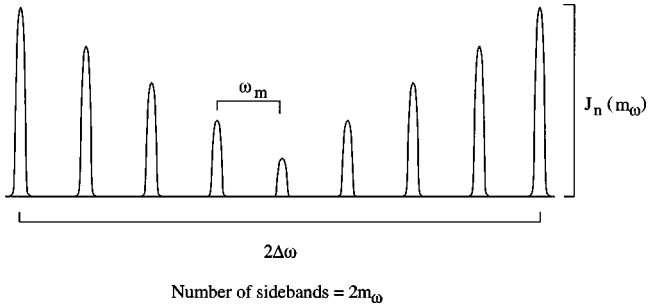

FIG. 3. A scheme of the sideband spectrum expected to be detected in the spectrum analyzer as a result of frequency modulation.

The frequency (in Hertz) of an ESR signal is proportional to the external magnetic field: $\upsilon(=\omega/2\pi)=[g\beta B]/h$, where g is the g value of the spin center, β is the Bohr magneton, B is the magnetic field (in Gauss), and h is Planck's constant. Ideally, one would like to change the magnetic field slowly and to observe the corresponding change in frequency. It is, however, difficult to keep the STM stable in these conditions. An alternative way is to modulate the magnetic field such that $B=B_0+\Delta B\cos(\omega_m t)$ and to detect the signal in frequency domain. B_0 is the unmodulated field, $2\Delta B$ is the peak-to-peak intensity of the modulation, and ω_m is the modulation frequency ($\omega_m=2\pi\upsilon_m$, where υ_m is in units of Hertz). The modulation must be faster than the response of the STM feedback loop. In these conditions, the frequency of the signal should become time dependent such that $\omega=\omega_0+\Delta\omega\cos(\omega_m t)$, where ω_0 is the unmodulated frequency and $\Delta\upsilon(=\Delta\omega/2\pi)=[g\beta\Delta B]/h$ is the frequency modulation intensity introduced by the field modulation.

In Ref. 7 we explained that when the frequency of a signal is modulated such that $\omega=\omega_0+\Delta\omega\cos(\omega_m t)$, then the signal detected by the spectrum analyzer shows a sideband spectrum with a very well-known structure (Fig. 3). The absolute magnitude spectrum observed is characterized by a set of equally spaced sidebands with frequencies $\omega_0,\omega_0+\omega_m,\omega_0-\omega_m,\omega_0+2\omega_m,\omega_0-2\omega_m,\ldots,\omega_0+n\omega_m,\omega_0-n\omega_m$. The intensity of the nth sideband is given by $J_n(m_\omega)$, where J_n is the nth-order Bessel function of the first kind, and m_ω is the modulation index ($=\Delta\omega/\omega_m$). The number of sidebands is roughly $2m_\omega$ and the total width of the sideband spectrum is $2\Delta\omega$. In the case when there are many closely spaced sidebands (large modulation index), it is no longer possible to distinguish between them. Nevertheless, the spectrum has a very special line shape, with a linewidth of $2\Delta\omega$. Such a spectrum is shown in Fig. 4 (bottom).

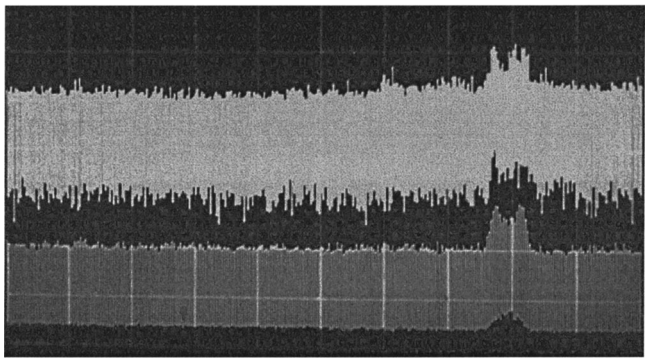

FIG. 4. An electron-spin-resonance (ESR)-STM spectrum taken with the spectrum analyzer alone. The analyzer total frequency scan was 5 MHz centered at 441 MHz. The trace in the top shows a line shape observed from the STM under conditions of field modulation. The bottom trace is the corresponding frequency modulated signal from a frequency synthesizer.

Figure 4 shows that also the electron-spin resonance (ESR)-STM signal from the iron atoms shows this particular line shape, which proves that indeed the frequency is time dependent due to the magnetic-field modulation $[\omega=\omega_0+\Delta\omega\cos(\omega_m t)]$. The upper trace is an electron-spin-resonance (ESR)-STM signal observed at a magnetic field of 152.5 G which corresponds to a frequency of 442 MHz (for $g=2.07$). The modulation frequency was 20 kHz and the field modulation intensity was $2\Delta B=82.5$ mG. This corresponds to $2\Delta\nu=240$ kHz, which is the total width of the sideband spectrum. A synthesized spectrum with these parameters is shown in the lower trace. The detection parameters in the spectrum analyzer (bandwidth, sweep time, etc.) were the same in both traces. Thus, these two traces are very similar. The similarity between them shows that indeed, the frequency depends in real time on the value of the magnetic field—also on the iron spin center.

Figure 5 shows two spectra that were recorded when the tip was tunneling above an island similar to those shown in Fig. 1. The spectra were recorded when the output of the spectrum analyzer was fed into a phase-sensitive detector.

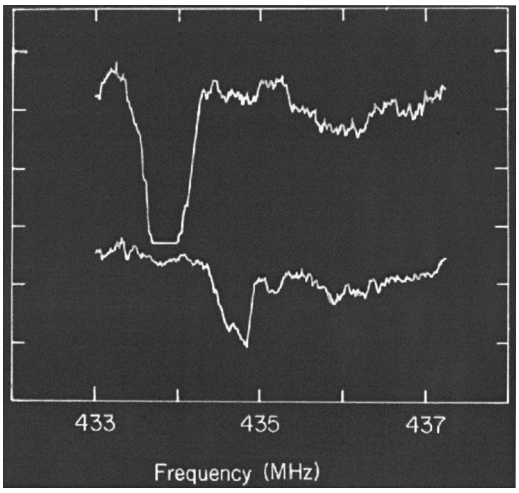

FIG. 5. Two electron-spin-resonance (ESR)-STM spectra at a frequency corresponding to $g=2.07$ with an absorption line shape as observed with a lock-in amplifier.

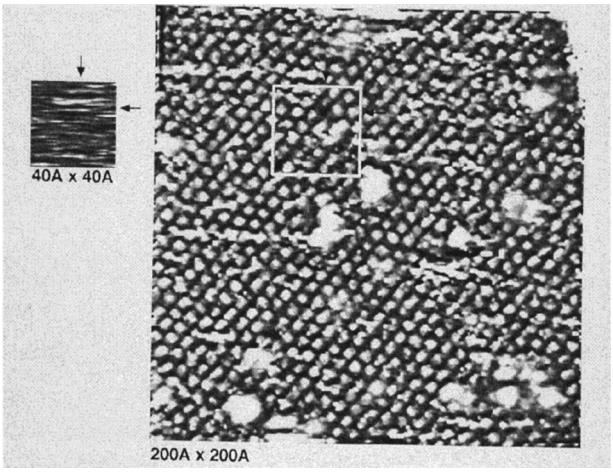

FIG. 6. A two-dimensional electron-spin-resonance (ESR)-STM image over a vacancy in a γ-$FeSi_2$ surface. The spectrum was recorded by looking at the output of the lock-in amplifier when the detection band of the spectrum analyzer is fixed at a single frequency corresponding to $g=2.07$. The phase (in the lock-in amplifier) of this spectrum is mainly positive (which corresponds to absorption line shape).

These spectra were recorded at the conditions of a modulation frequency of 20 kHz and a modulation intensity of $2\Delta B=50$ mG. The tunneling current was 0.2 nA. The magnetic field in these measurements was 150 G. Unlike the spectra that were reported in Ref. 7 these spectra have a clear absorption line shape rather then a derivative line shape. Both derivative and absorption line shapes were observed from both the Fe in silicon and the Si/SiO_2 systems. The absorption line shapes have a significant advantage that if it is possible to stabilize the tip above one position on the surface without drifting away, then several spectra like this can be added together—to improve the sensitivity. In the case of a derivative line shape, the spectral diffusion that may exist in the measurement will prevent improvement of the sensitivity when the spectra are added.

A two-dimensional electron-spin-resonance (ESR)-STM image is shown in Fig. 6. The experimental conditions are similar to those used in observing Fig. 5. The electron-spin-resonance (ESR)-STM spectrum in the left was taken from the area marked by a square in the topographic image in the right. The position from which the signal is observed is shown by two arrows. It corresponds to a surface position where a vacancy in the 2×2 reconstruction is located. This makes sense, since as was discussed earlier, the iron atoms are located in subsurface sites in these γ-$FeSi_2$ regions.

III. DISCUSSION

In order to demonstrate the circumstances in which derivative and absorption line shapes are expected in our detection system we have made a simulation of it using a MATLAB signal-processing software. First, a simulation of a spectrum analyzer has to be done. The spectrum analyzer is a tunable superheterodyne receiver. The input signal [initially a signal with a fixed frequency $\cos(\omega_0 t)$ is assumed] is mixed first with a frequency that is outside the frequency span of interest, and then a broadband filter (with the width of the

frequency span) is applied. This first mixing and filtering is known as image rejection. Afterwards, the signal is mixed again with a frequency that is the frequency of detection of the spectrum analyzer. This frequency (ω_d) is increasing linearly with time: $\omega_d=\omega_l+vt$, where ω_l is the detection frequency at $t=0$, and ω_l+vt_{sw} is the frequency at the moment the sweep is completed (t_{sw} is the sweep time of the analyzer). The output of this mixing is composed of both sum and difference frequencies between the detection frequency and the signal. To get rid of the fast harmonics, the signal is filtered with a narrow-band filter with a width that forms the resolution bandwidth of the spectrum analyzer. Mixing with two frequencies (rather than one) is required to destroy all the phase information in the signal in order to give the absorption line shape that is observed in the spectrum analyzer. At this stage, the signal is rectified and filtered again with a filter width corresponding to the video bandwidth in the spectrum analyzer. When a periodic signal is put in this virtual spectrum analyzer, one observes an absolute magnitude signal with a line shape identical to the one observed from a real spectrum analyzer; the line width is the resolution bandwidth. This required some adjustments: The simulated line shape is dependent to some extent on the exact nature of the digital filter that is used in the simulation. We have used filters that gave a line shape identical to what is observed with our spectrum analyzer.

Afterwards, the frequency of the signal is modulated such that $\omega=\omega_0+\Delta\omega\cos(\omega_m t)$, where ω_0 is the unmodulated frequency, $\Delta\omega$ is the modulation intensity, and ω_m is the modulation frequency, for simulating the effect of the field modulation. This introduces ω_m components in the response of the spectrum analyzer. In the experimental detection scheme, these components are detected with a phase-sensitive detector. To simulate this operation, the output of the spectrum analyzer is mixed with a reference wave $\cos(\omega_m t)$ and the result is filtered by a filter with a width that corresponds to the integration time constant (τ_{psd}) of the lock-in amplifier.

Linewidths to the signal were introduced in time domain by assuming that the signal has added some phase noise. The phase randomization times are randomly distributed around their average: the correlation time τ_c. We focus on the cases where the linewidth of the signal, as appears in the spectrum analyzer, is determined by its natural lifetime ($1/\tau_c > rbw$, where *rbw* is the resolution bandwidth of the spectrum analyzer). In these cases the phase of the signal seen in the phase-sensitive detector, depends on the ratio between the integration time (τ_{psd}) and the time it takes to sweep the linewidth. This makes sense, because when the bandwidth of the spectrum analyzer is at the lower frequency part of the line, the output of the spectrum analyzer creates a positive output in the phase-sensitive detector. When it is in the higher-frequency part of the line, this output will become negative. However, what happens when the integration time is so large that these two contributions mix together? The answer is shown in Fig. 7. The simulations were performed under the assumption that $rbw=SW/100$, namely, the resolution bandwidth is 1% of the total frequency span. As discussed in a previous paper (Ref. 7) the signal intensity is maximized when the modulation intensity is in the same magnitude as the resolution bandwidth. Therefore, we have assumed $\Delta\omega=rbw$ in the simulation. As discussed there, the

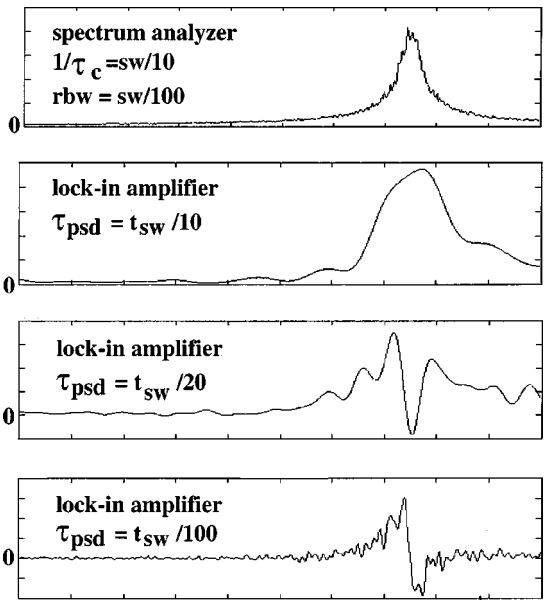

FIG. 7. A computer simulation showing the affect of increasing the integration time of the lock-in amplifier (τ_{psd}) on a signal with a finite lifetime. The upper trace shows the signal in the spectrum analyzer. The other three traces show the output in the lock-in amplifier for different values of τ_{psd}.

intensity of the first harmonic in the modulation frequency is maximized when $\Delta\omega/\omega_m=2$. At higher modulation indices, the intensity of the higher harmonics grow at the expense of the first one. Therefore, we assumed a modulation index of 2 in the simulation. However, the conclusions of the simulation are valid also in cases where we did not make these assumptions.

The line shape as seen with the spectrum analyzer is shown in Fig. 7 (top). Since the natural linewidth is assumed to be much larger than both the modulation intensity and the resolution bandwidth, the effect of the modulation is not seen in the simulated spectrum analyzer line shape. Nevertheless, when the time dependent output of the analyzer is put into a lock-in amplifier, the observed line shape depends on the ratio between the time it takes to sweep the linewidth (approximately 10% of the total sweep time t_{sw}) and the integration time of the lock-in amplifier. When the later is much smaller ($\tau_{psd}=t_{sw}/100$) the observed line shape is approximately the derivative of the line shape of the spectrum analyzer. Thus, if a derivative line shape is observed, it is quite reasonable to assume, that its linewidth represents the natural linewidth of the signal. However, as the integration time of the lock-in amplifier increases, the line shape is gradually turned into an absorption line shape, and the linewidth no longer represents the natural line shape of the signal. It is important to emphasize that in these cases, the line shape can fluctuate much more than in the derivative line shape case.

The observation of an absorption line shape from the phase-sensitive detector in the simulation (and in the experiment) needs further clarification. As explained in Ref. 7 our detection system is expected to give a derivative of the line shape that is observed in the spectrum analyzer. Thus if the line shape is symmetric, when τ_{psd} is increased, the signal should completely disappear. However, normally the line shape is not symmetric since the spectrum analyzer has a

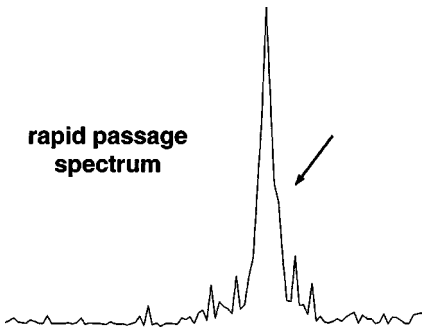

FIG. 8. A simulated asymmetric spectrum analyzer line shape observed at rapid passage conditions.

finite sweep time. The line shape is expected to be more asymmetric as the sweep velocity increases (rapid passage). Figure 8 shows a typical line shape under rapid passage conditions, when the sweep is done from left to right. The sweep is much faster than in Fig. 7 (top). It is clear that the slope at the left side of the line is larger than at the right side (marked by an arrow). Due to the rapid sweep, the modulation is added to a time-dependent linear sweep that distorts the line shape. This is quite similar to the asymmetric rapid passage line shapes detected, for example, in cw nuclear magnetic resonance.[19] A derivative of this line will be also asymmetric with a larger positive part. Therefore, a large value of τ_{psd} should give an absorption line shape in the phase-sensitive detector with a positive phase as is indeed observed. Even if the line shape in the spectrum analyzer is largely symmetric (such as in Fig. 7 (top)), still, the symmetric part is eliminated by phase-sensitive detection, and the asymmetric part will give an absorption line shape. A detailed quantitative study regarding the observation of absorption line shapes is currently performed.

In our electron-spin-resonance (ESR)-STM experiments we observed different line shapes that are similar to either of the spectra shown in Fig. 7. Coming back to the experimental data shown here, the time constant of the lock-in amplifier (τ_{psd}) that was used to observe the spectrum in Fig. 5, was 0.3 s, while the total sweep time was 30 s (to sweep 5 MHz). It is thus possible to say something about the order of magnitude of the τ_c of the signal observed experimentally, but in order to measure it precisely, a derivative line shape is required. For this, the value of τ_{psd} has to be reduced.

To summarize, we have shown that the electron-spin-resonance (ESR)-STM can be performed on surfaces where atomic resolution is observed, and that spin centers with a g value different than 2 can be detected. We have also explained the occasional appearance of absorption line shapes when a phase-sensitive detector is used. However, the sensitivity problem has not been solved yet. A possible solution will be to detect the signal in the time domain, as done in a similar way in modern magnetic resonance spectrometers, and to work at cryogenic temperatures to minimize the thermal noise. Also, the question of the precise mechanism of this phenomenon has still to be resolved.

ACKNOWLEDGMENTS

This work was supported by the German Israeli Binational Foundation for Research and Development (GIF). Additional support was given by grants from the Israel Science Foundation (ISF) and from Intel.

[1] J. Koehler, J. A. J. M. Disselhorst, M. C. J. M. Donckers, E. J. J. Groenen, J. Schmidt, and W. E. Moerner, Nature (London) **363**, 342 (1993).
[2] J. Wrachtrup, C. von Borczyskowski, J. Bernard, M. Orrit, and R. Brown, Nature (London) **363**, 344 (1993).
[3] J. Wrachtrup, C. von Borczyskowski, J. Bernard, M. Orrit, and R. Brown, Phys. Rev. Lett. **71**, 3565 (1993).
[4] D. Rugar, C. S. Yannoni, and J. A. Sidles, Nature (London) **360**, 563 (1992).
[5] Y. Manassen, R. J. Hamers, J. E. Demuth, and A. J. Castellano Jr., Phys. Rev. Lett. **62**, 2531 (1989).
[6] Y. Manassen, E. Ter-Ovanesyan, D. Shachal, and S. Richter, Phys. Rev. B **48**, 4887 (1993).
[7] Y. Manassen, J. Magn. Reson. **126**, 133 (1997).
[8] A. W. McKinnon and M. E. Welland (unpublished).
[9] H. H. Woodbury and G. W. Ludwig, Phys. Rev. **117**, 102 (1960).
[10] M. Berke, E. Weber, H. Alexander, H. Luft, and B. Elschner, Solid State Commun. **20**, 881 (1976).
[11] A. L. Vazquez de Parga, J. de la Figuera, O. Ocal, and R. Miranda, Europhys. Lett. **18**, 595 (1992).
[12] H. von Känel, K. A. Mäder, E. Müller, N. Onda, and H. Sirringhaus, Phys. Rev. B **45**, 13 807 (1992).
[13] W. Raunau, H. Niehus, T. Schilling, and G. Comsa, Surf. Sci. **266**, 203 (1993).
[14] N. E. Christensen, Phys. Rev. B **42**, 7148 (1990).
[15] P. A. Bennet, D. G. Cahill, and M. Copel, Phys. Rev. Lett. **73**, 452 (1994).
[16] N. Motta, A. Sgarlata, G. Gaggioti, F. Patella, A. Balzarotti, and M. de Crescenzi, Surf. Sci. **284**, 2578 (1993).
[17] T. Miki, Y. Matsui, K. Matsubara, and K. Kishimoto, J. Appl. Phys. **75**, 1693 (1994).
[18] Y. Manassen, I. Mukhopadhyay, and G. Pchelarov (unpublished).
[19] B. A. Jacobsohn and R. K. Wangness, Phys. Rev. **73**, 942 (1948).